



# Lawrence Berkeley Laboratory

UNIVERSITY OF CALIFORNIA

## Materials & Chemical Sciences Division

RECEIVED  
LAWRENCE  
BERKELEY LABORATORY

MAR 4 1988

LIBRARY AND  
DOCUMENTS SECTION

### The Morphological Stability of Continuous Intergranular Phases: Thermodynamic Considerations

W.C. Carter  
(M.S. Thesis)

December 1987

**TWO-WEEK LOAN COPY**

*This is a Library Circulating Copy  
which may be borrowed for two weeks.*



LBL-24695

## **DISCLAIMER**

This document was prepared as an account of work sponsored by the United States Government. While this document is believed to contain correct information, neither the United States Government nor any agency thereof, nor the Regents of the University of California, nor any of their employees, makes any warranty, express or implied, or assumes any legal responsibility for the accuracy, completeness, or usefulness of any information, apparatus, product, or process disclosed, or represents that its use would not infringe privately owned rights. Reference herein to any specific commercial product, process, or service by its trade name, trademark, manufacturer, or otherwise, does not necessarily constitute or imply its endorsement, recommendation, or favoring by the United States Government or any agency thereof, or the Regents of the University of California. The views and opinions of authors expressed herein do not necessarily state or reflect those of the United States Government or any agency thereof or the Regents of the University of California.

The Morphological Stability of Continuous Intergranular Phases:  
Thermodynamic Considerations

W. Craig Carter

M.S. Thesis

Lawrence Berkeley Laboratory  
University of California  
Berkeley, California 94720

This work was supported by the U.S. Department of Energy under  
Contract Number DE-AC03-76SF00098.

## **Acknowledgements**

First and foremost, my heartfelt gratitude and respect belongs to Andy Glaeser. Without his extreme patience and keen insight, this manuscript would certainly never have been written. He is a great friend and mentor.

Rowland Cannon has earned my appreciation. Never has anyone challenged me so much; and never has there been a more natural teacher. His passion for science is an inspiration.

John Salmon, Lorenzo Sadun and John Cahn each contributed very useful discussions and improved this thesis significantly.

I thank Alan Searcy and Didier deFontaine for reading this manuscript.

Last and utmost, my love and respect belong to my partner in life and crime. Because Marty loves me in spite of all my foibles, she deserves my gratitude more than anyone. I love her dearly.

*"But then, Mr. Finn, there is such a difference between  
life and theory; -- is there not?"*

*"And it is so comfortable to have theories that one  
is not bound to carry out," said Phineas.*

Anthony Trollope, from  
*Phineas Finn*  
page 404, Penguin Books

## 1. INTRODUCTION

Rayleigh presented the first complete analysis of the morphological instability of continuous phases in 1878.<sup>1</sup> As Rayleigh remarked, "[these] phenomena, interesting not only in themselves, but also as throwing light upon others yet more obscure, depend for their explanation upon the transformations undergone by a [cylindrical body] when slightly displaced from its equilibrium configuration and left to itself".<sup>2</sup> The Rayleigh analysis indicates that infinitesimal periodic perturbations with a wavelength,  $\lambda$ , exceeding  $2\pi R$  (the cylinder circumference) will reduce the specific (per unit volume) surface energy, and thus will increase in amplitude. Growth of perturbations with  $\lambda > \lambda_{\min}(= 2\pi R)$  eventually cause the formation of one discrete particle per wavelength increment of cylinder.

Such phenomena continue to be the subject of considerable interest; a wide range of microstructural phenomena involving capillarity-induced shape changes have been analyzed or modeled by a Rayleigh analysis. These include: the stability of lamellar eutectics,<sup>3-5</sup> fibers in composites,<sup>6</sup> and artificially lengthened precipitates,<sup>7-8</sup> the shape evolution of field ion emitter tips,<sup>9,10</sup> healing of cracks introduced by thermal shock,<sup>11,12</sup> as well as by scoring and welding of bicrystals,<sup>13,14</sup> and the stability of the continuous pore phase during sintering of powder compacts.<sup>15,16</sup>

The Rayleigh analysis permits qualitative understanding of many of these phenomena, however, complications arise when the continuous phase is located at a grain boundary. For an intergranular phase, each grain boundary intersection is characterized by some dihedral angle. The associated deviation from a cylindrical geometry changes both the surface energy per unit volume and the stability condition.

The modifying effect of dihedral angle on the stability of continuous grain boundary phases was recognized by C. S. Smith.<sup>17</sup> In discussing continuous phases along three grain junctions Smith wrote, "If a second phase forming at a grain edge has a dihedral angle against grain boundaries of nearly  $180^\circ$ , it will behave like a cylinder and will certainly break up. If, however, the interphase tension is low in comparison with the adjacent grain boundary

tension, the resulting triangular shape becomes stable at longer and longer lengths until, at a dihedral angle of  $60^\circ$  and below, the phase becomes stable at any length of grain edge."

The stability of continuous phases along three grain junctions of tetrakaidecahedral grains has been evaluated by both Beere<sup>18,19</sup> and Tucker and Turnbull.<sup>20</sup> These analyses indicate the important modifying effect of dihedral angle on intergranular phase continuity conditions. More generally, continuous phases may be situated at (along) the junctions of an arbitrary number of grains. The ensuing analysis quantifies the discussion of Smith by extending Rayleigh's method to continuous phases surrounded by  $n$  grains with (variable) dihedral angle  $\psi$ . Results indicate the stability condition depends strongly on the intergranular phase geometry (as dictated by the values of  $n$  and  $\psi$ ), and may differ significantly from that of a cylinder.

A complete analysis of morphological instability has two components:<sup>21</sup> a thermodynamic analysis identifying the smallest wavelength (infinitesimal amplitude) perturbation for which the amplitude will increase, and a kinetic analysis determining the particular wavelength for which perturbation growth is most rapid. A thermodynamic analysis for non-faceting surfaces with single-valued interfacial tensions is presented here. Possible modifications resulting from surface faceting<sup>22,23</sup> and the implications of the analysis to the kinetics of phase breakdown have been discussed elsewhere.<sup>23</sup>

## 2. THEORETICAL ANALYSIS: DETERMINATION OF $\lambda_{\min}$

In this section, the briefest outline of the analysis of  $\lambda_{\min}$  is presented. The interested reader is referred to appendix I for a detailed account of the involved mathematics.

The objectives are the calculation of the surface area and volume of both a perturbed and unperturbed channel as a function of the number of bounding grains  $n$ , and the dihedral angle  $\psi$ . The results of these calculations are employed to define the condition for thermodynamic stability of a continuous grain boundary phase.

### 2.1. Analysis

Figure 1 illustrates most of the geometrical parameters relevant to the analysis. Isotropic interfacial energies (grain boundary and interphase) are assumed, i.e., the energy for each type of interface has some unique but constant value. Each interphase boundary will thus have identical curvature, and intersect the adjoining interphase boundaries at a common dihedral angle,  $\psi$ . The intergranular phase will display  $n$ -fold symmetry. The channel cross-section may be circumscribed by a circle of radius  $R_c$ , which intersects all  $n$  triple junctions. Let the radius of curvature for any side be  $\rho'$ , then it is possible to describe one of the surfaces by:

$$(x + \eta)^2 + y^2 = \rho'^2 \quad (2.1)$$

within  $-\frac{\pi}{n} \leq \theta \leq \frac{\pi}{n}$ .  $\eta'$  is the distance between the center of the particular circular arc and the origin.

Normalizing,

$$\rho \equiv \frac{\rho'}{R_c} \quad \text{and} \quad \eta \equiv \frac{\eta'}{R_c} \quad (2.2)$$

A perturbation on the cross-section can be described as the largest term of some periodic function of wavelength  $\lambda$  and arbitrarily small amplitude  $\delta$ .

$$R_c = R_o + \delta \cos kz \quad (2.3)$$

where  $k \equiv \frac{2\pi}{\lambda}$ .

The surface excess energy per wavelength is:

$$f = \gamma_s A_s + \gamma_{gb} A_{gb} \quad (2.4)$$

where  $A_s$  is the surface area per wavelength, and  $A_{gb}$  is the grain boundary area.

The expressions for the surface and grain boundary area may be computed for arbitrary  $\psi$  and  $n$ .

$$A_{gb} = \frac{2n\pi}{k}(\alpha - R_o) \quad (2.5)$$

where  $\alpha$  is an arbitrary boundary length.

$$A_s = \frac{2n\pi R_o}{k} \left[ U + \frac{\delta^2 k^2}{4} P \right] \quad (2.6)$$

where,

$$U = 2\rho \left[ \frac{\pi}{n} - \frac{\pi}{2} + \frac{\psi}{2} \right] \quad (2.7)$$

and

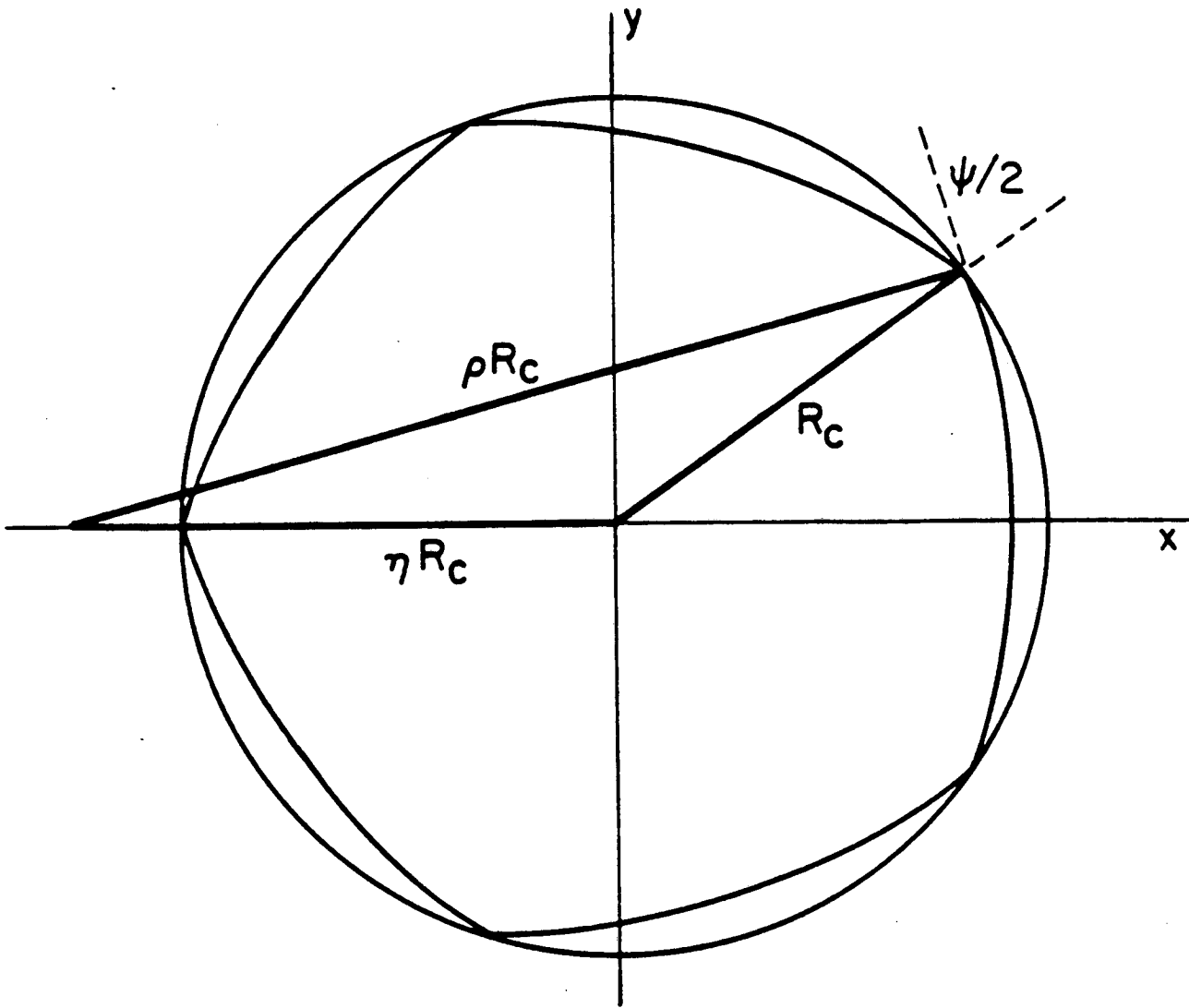
$$P = (2\rho^3 + \rho\eta^2) \left( \frac{\pi}{n} + \frac{\psi}{2} - \frac{\pi}{2} \right) + \quad (2.8)$$

$$\cos\left(\frac{\psi}{2}\right) \left( 5\eta\rho^2 \cos\left(\frac{\pi}{n}\right) - 2\eta^3 \sin^2\left(\frac{\pi}{n}\right) \cos\left(\frac{\pi}{n}\right) - \eta^2 \rho \sin\left(\frac{\psi}{2}\right) - 2\rho^3 \sin\left(\frac{\psi}{2}\right) - 2\rho^3 \sin^3\left(\frac{\psi}{2}\right) \right)$$

The volume per wavelength may also be computed:

$$V_p = \frac{\pi V_u}{k} (2R_o^2 + \delta^2) \quad (2.9)$$

where  $V_u$  is a geometric factor.



XBL861-7403

Figure 1

Expanding the surface excess energy, eq. (2.4), with the constraint of constant volume:

$$f = \gamma_s \left[ \frac{4n \pi \cos(\frac{\psi}{2}) \alpha}{k} + \frac{2n \pi}{k} \left[ \frac{kV_p}{2\pi V_u} \right]^{1/2} U - \frac{4n \pi \cos(\frac{\psi}{2}) \alpha}{k} \cos(\frac{\psi}{2}) \left[ \frac{kV_p}{2\pi V_u} \right]^{1/2} \right] + \quad (2.10)$$

$$\gamma_s \frac{n \pi}{k} \left[ \frac{kV_p}{2\pi V_u} \right]^{1/2} \left[ 2 \cos(\frac{\psi}{2}) - U + \left[ \frac{kV_p}{2\pi V_u} \right] k^2 P \right] \frac{\delta^2}{2}$$

As in all problems of metastability, stability is determined by the sign of the second derivative, i.e., the term multiplying  $\frac{\delta^2}{2}$ . Thus, the channel is unstable to all infinitesimal perturbations with wavelengths  $\lambda > \lambda_{\min}$  for which the term which multiplies  $\delta^2$  is negative. Finally, the equation

$$\lambda_{\min} = 2\pi R_o \left[ \frac{P}{U - 2 \cos(\frac{\psi}{2})} \right]^{1/2} \quad (2.11)$$

defines a critical condition for perturbation growth. It is analogous to the Rayleigh result for the cylinder.

The  $\cos \frac{\psi}{2}$  term stems from the change in grain boundary area. Only dihedral angles in the range,  $0 < \psi \leq \pi$ , are considered,  $\cos \frac{\psi}{2}$  is always positive. For  $\psi$  between 0 and  $\pi$ , both P and U are positive. Thus, the change in grain boundary area accompanying development of a perturbation increases  $\lambda_{\min}$  and stabilizes the intergranular phase.

## 2.2. End-State Calculations

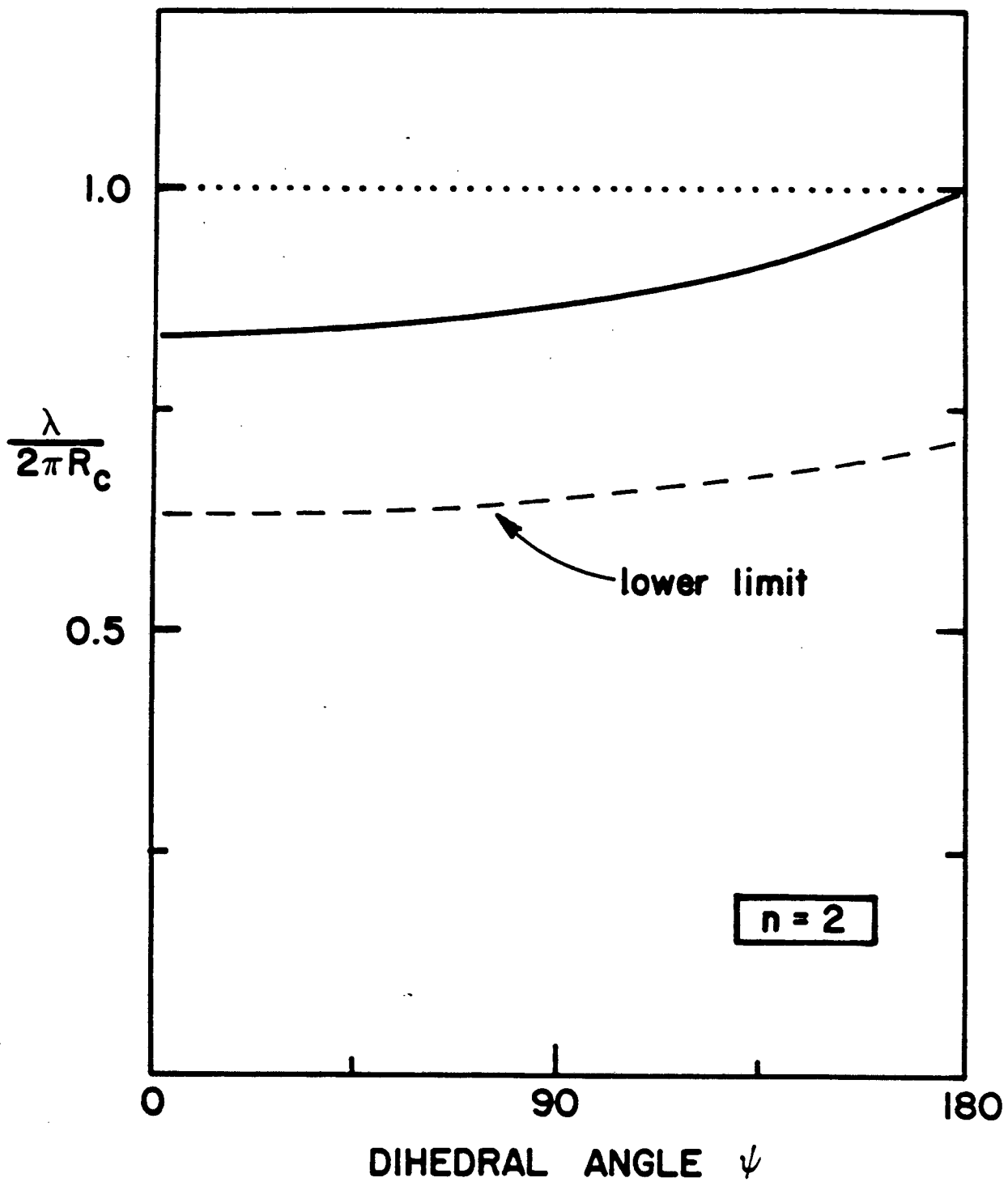
The stability condition derived in this analysis defines the minimum wavelength necessary for an infinitesimal periodic perturbation on  $R_o$  to increase in amplitude. Infinitesimal perturbations with  $\lambda > \lambda_{\min}$  decrease the interfacial energy in comparison to that of an unperturbed cylinder having the same volume per wavelength. Wavelengths less than  $\lambda_{\min}$  can grow for large perturbations.<sup>24</sup>

The interfacial area of the perturbed channel is sensitive to the form of the imposed perturbation. Conceivably, a perturbation with an additional radial or rotational component could yield a smaller  $\lambda_{\min}$  than derived here. Hence, although the calculated values for  $\lambda_{\min}$  presented serve as a sufficient condition for instability, perturbations of greater geometrical complexity may provide a smaller value for  $\lambda_{\min}$  as a necessary condition for instability.

Accordingly, it is desirable to determine a lower limit wavelength  $\lambda_{//}$  as a function of  $\psi$  and  $n$ . This entails calculating the perturbation wavelength for which the total (grain boundary and interphase boundary) interfacial energy per wavelength in the unperturbed and final (discrete particle) states are equal (Appendix II). Shorter wavelength perturbations would increase total interfacial energy. Thus, the difference between  $\lambda_{//}$  and  $\lambda_{\min}$  indicates the maximum possible reduction in  $\lambda_{\min}$  achievable by imposition of a more geometrically complex or large perturbation.

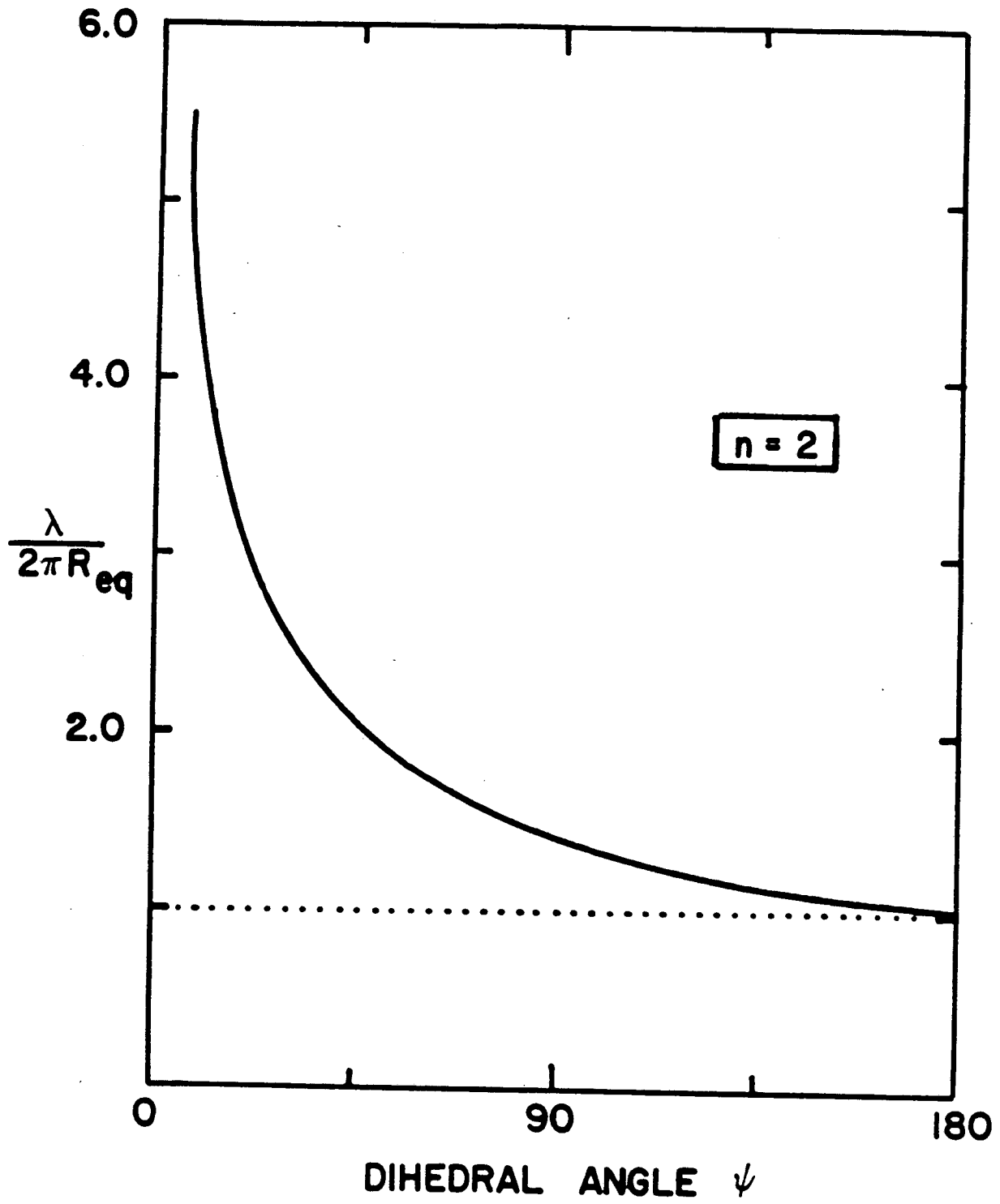
The calculation is straightforward for  $\psi = \pi$ , since this implies  $\gamma_{gb} = 0$ , and consequently, changes in grain boundary area accompanying the transition from a cylinder to an ensemble of equidistant spheres of equivalent total volume need not be considered.<sup>a</sup> For the simple case of a cylinder,  $\lambda_{//} = \frac{9}{2}R_o$  independent of  $n$ . For  $\psi < \pi$ , the calculation is more tedious. Results for  $n = 2$  and  $n = 3$  are present in Figs. 2a and 3a, respectively. For  $n = 3$ , results of Clemm and Fisher<sup>25</sup> were used to describe the geometry of the discrete phase. The generalization to arbitrary  $n$  and results for  $n > 3$  will be presented elsewhere.<sup>24</sup>

<sup>a</sup>Comparison of end-state calculations for  $n = 2, 3$  including and excluding grain boundary area changes indicate a trend similar to that suggested by Eq. 2.11, i.e., the grain boundary area changes associated with an infinitesimal perturbation increase  $\lambda$ , and stabilize the continuous phase.



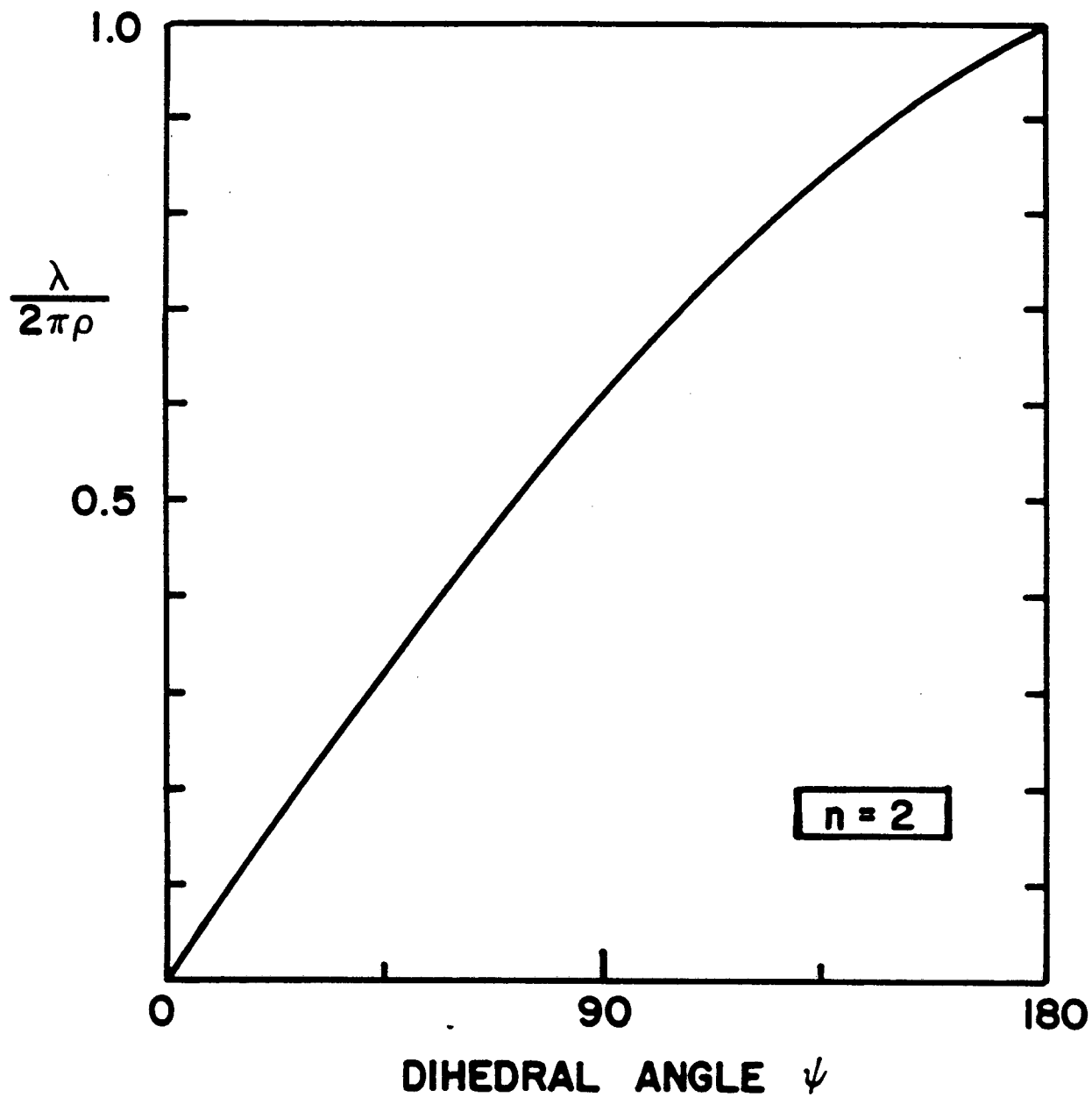
XBL 866-2327

Figure 2a



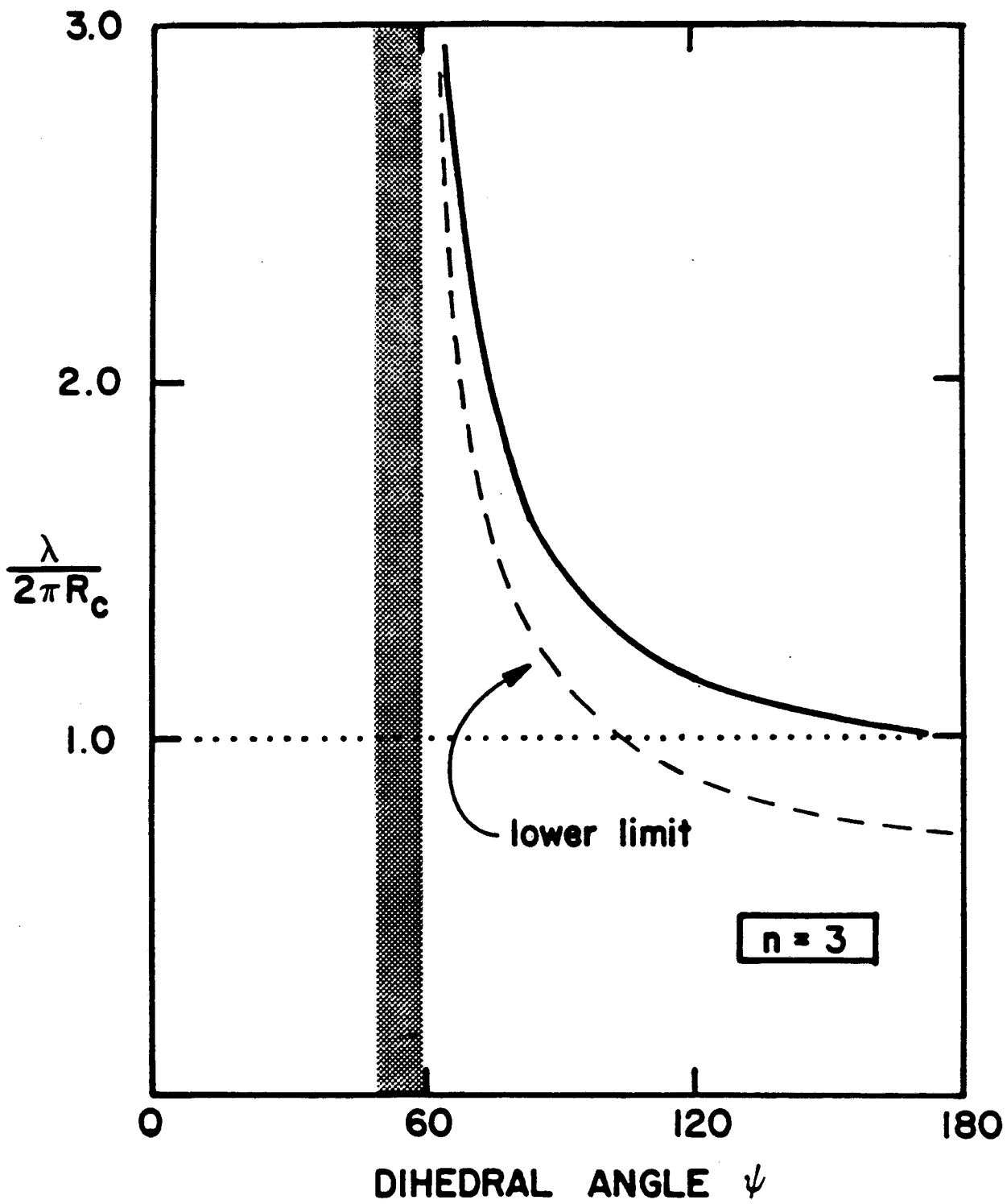
XBL 866-2328

Figure 2b



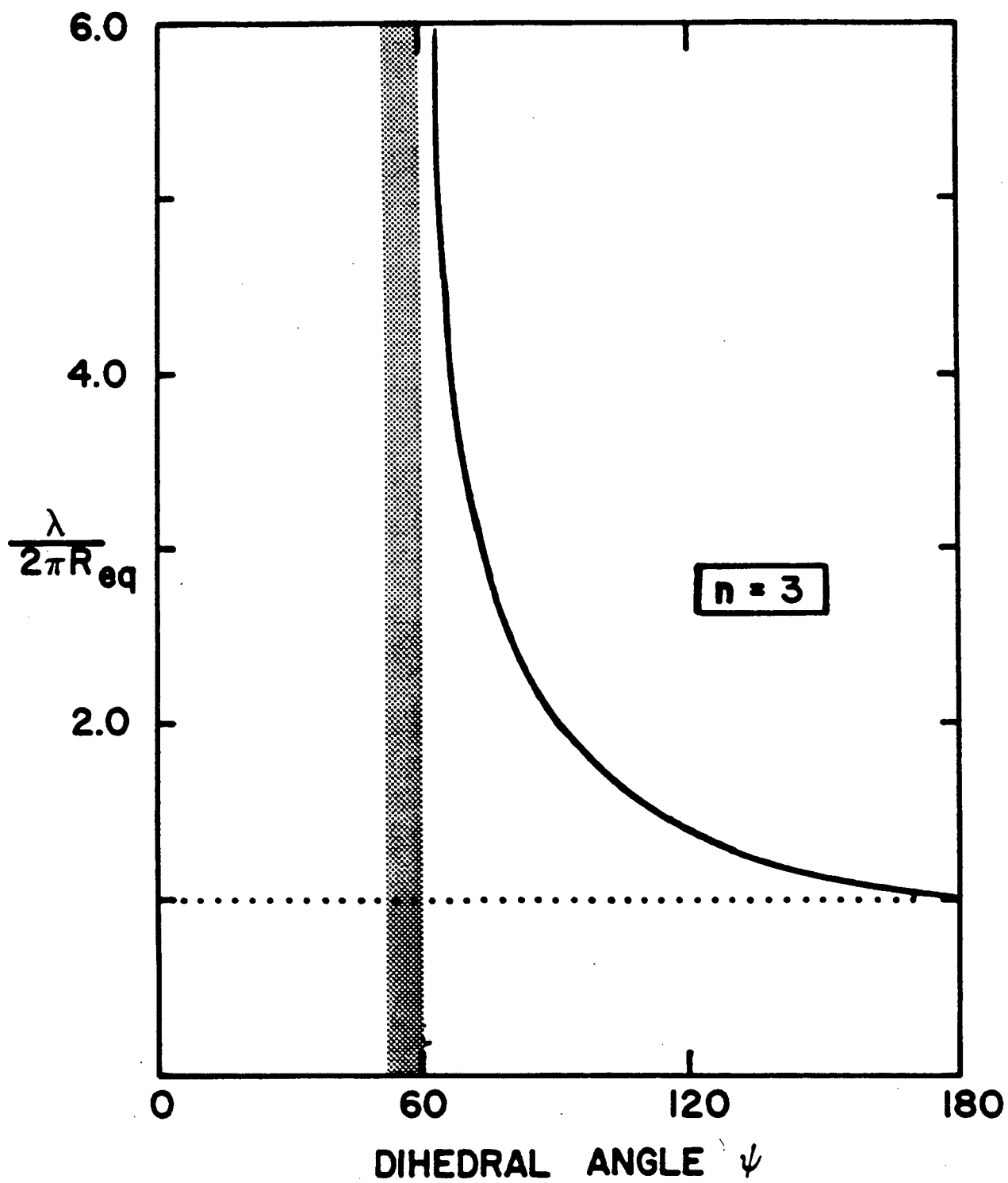
XBL 866-2329

Figure 2c



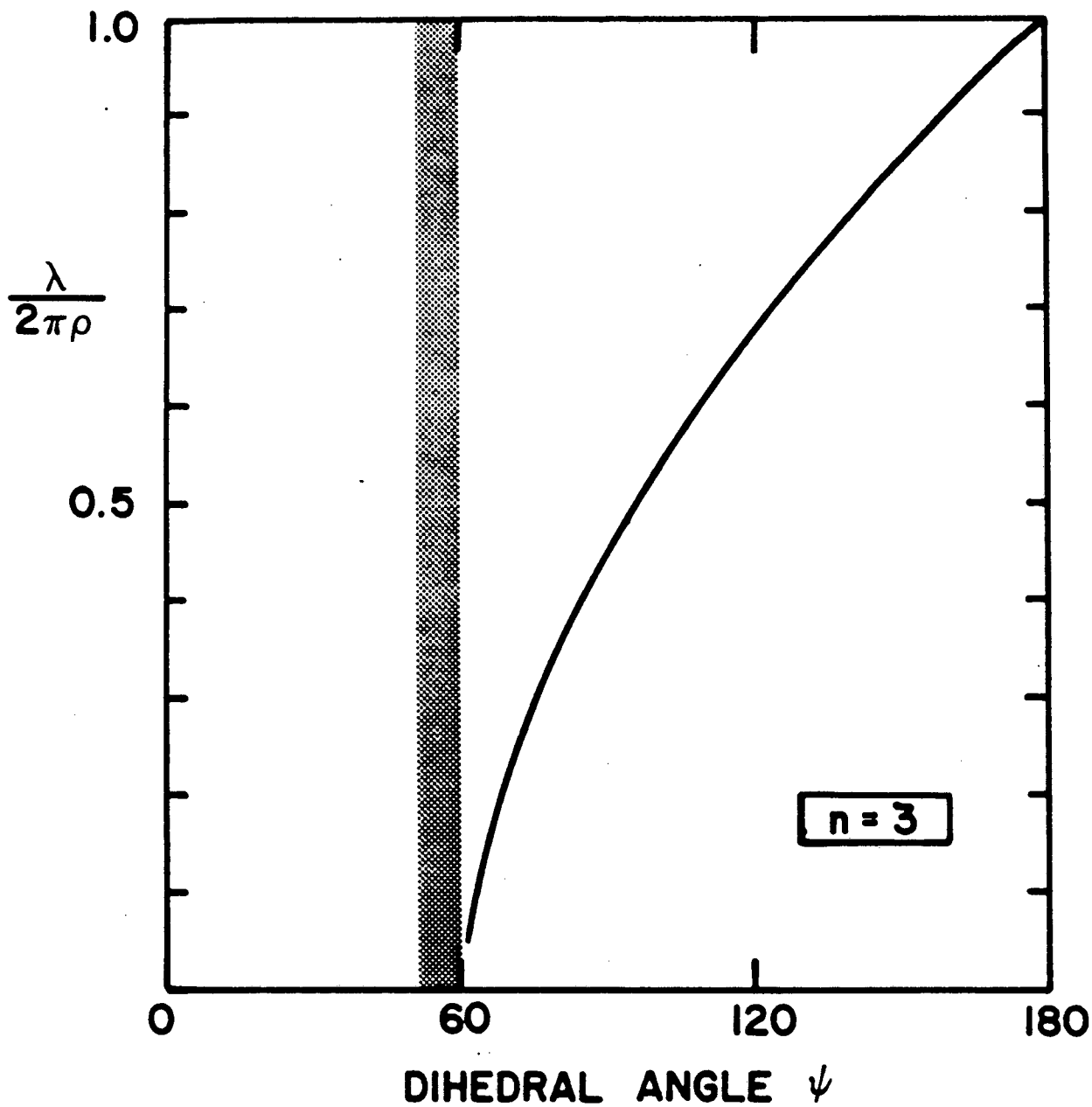
XBL 866-2330

Figure 3a



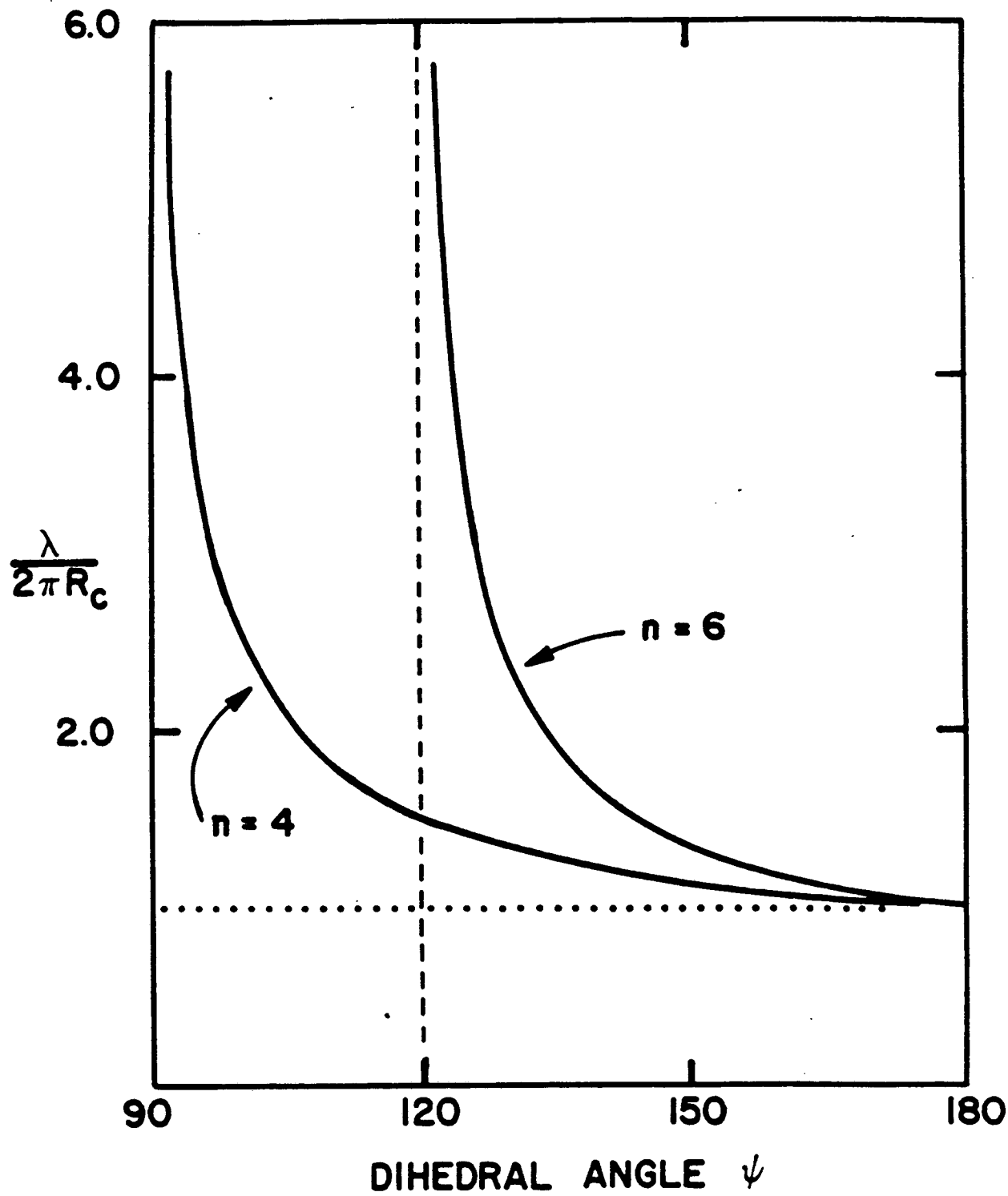
XBL 866-2332

Figure 3b



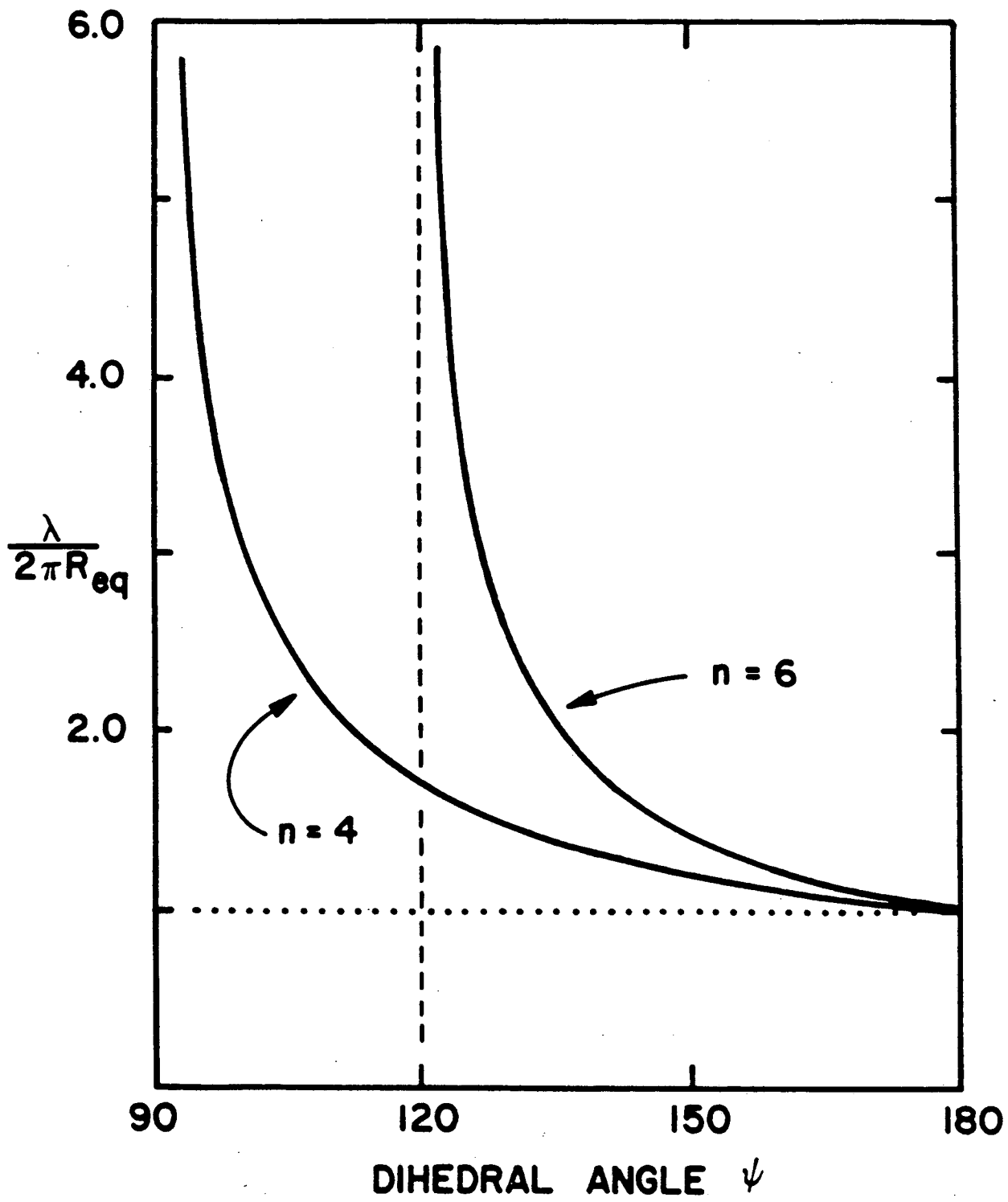
XBL 866-2331

Figure 3c



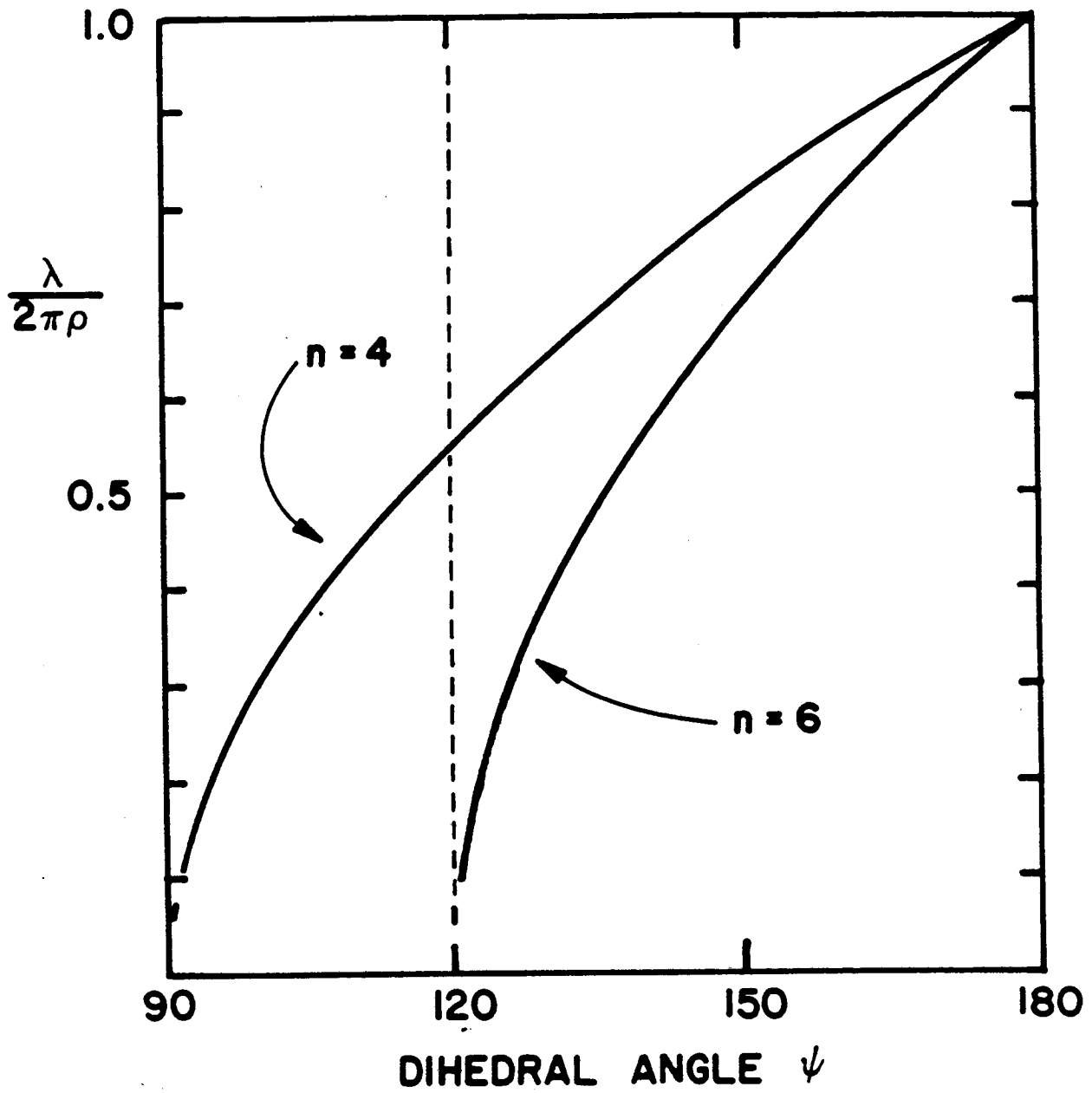
XBL 866-2333

Figure 4a



XBL 866-2334

Figure 4b



XBL 866-2335

Figure 4c

### 3. DISCUSSION

Results of the analysis for several  $n$  are presented in Figures 2-4. For each  $n$  (Figures 2a-4a),  $\lambda_{\min}$  coincides with the Rayleigh result ( $2\pi R_c$ ) for  $\psi = 180^\circ$ . For  $n = 2$ , the ratio  $\frac{\lambda_{\min}}{2\pi R_c}$  is  $< 1$  for all  $\psi < 180^\circ$ , decreasing with  $\psi$  to a limit of  $(\frac{7}{10})^{1/2}$  as  $\psi \rightarrow 0$ . The corresponding end state calculation (see Appendix II) for  $n = 2$  indicates that  $\lambda_{II}$  follows a similar trend, decreasing from 0.716 at  $\psi = 180^\circ$  to 0.633 when  $\psi = 0$ . The present values of  $\frac{\lambda_{\min}}{2\pi R_c}$  are lower than those appropriate to a sinusoidal perturbation imposed on  $\rho$ ,<sup>23</sup> and thus more closely approach a necessary condition for instability. The close correspondence between  $\lambda_{\min}$  and  $\lambda_{II}$  suggests that although a further reduction in  $\lambda_{\min}$  is possible, the decrease is likely to be small.

For  $n \geq 3$ ,  $\lambda_{\min}$  and  $\frac{\lambda_{\min}}{2\pi R_c}$  tend to infinity as  $\psi \rightarrow \pi - \frac{2\pi}{n}$ , or equivalently, as the interface curvature vanishes. The end state calculation ( $n = 3$ ) shows a similar increase in  $\lambda_{II}$  as  $\psi$  decreases from  $180^\circ$  to  $60^\circ$ . A previous analysis indicated a similar trend but a more rapid increase in  $\frac{\lambda_{\min}}{2\pi R_c}$  with decreasing  $\psi$ .<sup>23</sup> For fixed  $n$ , a continuous phase with lower  $\psi$  is expected to be more stable than one with higher  $\psi$ . For  $n \geq 3$ , the phase is completely stable to (infinitesimal) perturbations when  $\psi \leq \pi - \frac{2\pi}{n}$ . For fixed  $\psi$ , the stability increases with  $n$  (Table I).

To compare this analysis and that of Rayleigh, two normalization parameters are introduced. Defining  $R_{eq}$  as the cylinder radius yielding the same volume per unit length as an intergranular phase characterized by a dihedral angle  $\psi$ , the ratio  $\frac{\lambda_{\min}}{2\pi R_{eq}}$  normalizes the actual  $\lambda_{\min}$  by the minimum wavelength that would grow in a geometrically similar compact with an equivalent volume fraction of (cylindrical) second phase. The dependence of  $\frac{\lambda_{\min}}{2\pi R_{eq}}$  on  $\psi$  for various  $n$  is presented in Figs. 2b-4b.

An alternative normalization mode is based on consideration of the surface curvature as characterized by  $\rho$ . The stability condition of the intergranular phase may be compared with that of a cylinder having the same curvature, i.e., one with radius  $\rho$ . The results of this comparison, presented in Figs. 2c-4c, indicate the approximation  $\lambda_{\min} \approx 2\pi\rho$  overestimates  $\lambda_{\min}$  for all  $\psi < 180^\circ$  and becomes progressively poorer as  $\psi$  decreases.<sup>3</sup>

### 3.1. General Considerations:

The composition, inherent properties, morphology, and spatial distribution of a second phase within a matrix, can have an important impact on a material's ultimate properties. The incorporation of continuous filaments into polycrystalline matrices may dramatically alter mechanical behavior. High temperature stability and useful lifetimes of such composites will be influenced by the fibers' relative susceptibility to morphological instabilities and concurrent coarsening.<sup>3</sup> Continuous phases may provide high diffusivity transport paths, (e.g., vapor transport along continuous pore channels in  $\text{UO}_2$  fuel elements<sup>20</sup>) or be preferentially leached, thus limiting the utility of a material in storage applications, e.g., containment of nuclear waste. In these cases as well as others, factors influencing the morphological stability of continuous phases may become important considerations in materials design. The stabilizing effect of the dihedral angle is discussed below for specific cases.

### 3.2. Consideration of $n = 2$

Crack healing experiments have been conducted on cracked sapphire single crystals,<sup>13</sup> bicrystals,<sup>14</sup> and thermally shocked polycrystals<sup>11</sup> and used to determine surface diffusivities in alumina. During annealing, the crack first breaks down into parallel, high aspect ratio pore channels. These channels in turn undergo a Rayleigh instability, resulting in breakup into a

<sup>3</sup>In comparing normalizations, the trend  $\frac{\lambda_{\min}}{2\pi R_c}$  is simply a consequence of having  $\rho > R_c > R_{eq}$  when  $\psi < 180^\circ$ .

string of equidistant isolated pores. The ratio of pore spacing ( $\lambda$ ) to (apparent) pore radius  $r_p$  differs for surface diffusion and volume diffusion controlled breakup; the pore radius  $r_p$  and an experimentally measured breakup (ovulation) time are used to determine the appropriate diffusivity.

The dihedral angle will affect the shapes of both the continuous and discrete pores, and through its effect on  $\lambda_{\min}$ , will also affect the kinetically dominant wavelength, and thus both the size and spacing of discrete particles or phases resulting from perturbation growth processes. Experiments on a series of bicrystals with a systematic variation in  $\psi$  (owing to misorientation effects) would be expected to reveal a systematic variation in particle size and spacing. In polycrystals, incorporating a spectrum of  $\psi$ , "scatter" in the sizes and spacings of discrete particles would be observed. In polycrystalline alumina,<sup>11</sup> the pore spacing to pore diameter ratio varied by as much as factor two. Similar variability was obtained for the breakdown of elongated bubbles (appearing to lie on two grain interfaces) in tungsten filaments.<sup>8</sup>

For alumina, surface diffusion was identified as the dominant transport process in each case. However, the deduced surface diffusivities differ by between one and two orders of magnitude at the same temperature. An assessment of the contribution to scatter owing to dihedral angle effects is therefore of interest.

Since the shapes of both the pore channel and the isolated pores are affected by  $\psi$ , it is anticipated that  $\frac{\lambda}{2r_p}$  will also be dihedral angle dependent. For constant  $\frac{\lambda}{R_c}$ ,  $\frac{\lambda}{2r_p}$  decreases by  $\approx 4\%$  as  $\psi$  varies from  $180^\circ$  to  $0$  (Appendix III). Recent dihedral angle measurements in alumina by Handwerker<sup>26</sup> have indicated a wide dihedral angle range,  $85^\circ$  to  $170^\circ$ . Within this range of  $\psi$ , there is a factor  $\sqrt{2}$  decrease in  $\lambda_{\min}$ . The total "scatter" in  $\frac{\lambda}{2r_p}$  will depend on the dihedral angle dependence of the kinetically dominant wavelength. If the kinetically dominant wavelength is a mechanism dependent, but dihedral angle independent multiple of  $\lambda_{\min}$ , the total scatter in  $\frac{\lambda}{2r_p}$  owing to dihedral angle effects is  $< \pm 10\%$  and similar  $\frac{\lambda}{2r_p}$  ratios would be obtained regardless of whether measurements were conducted on single

crystals or polycrystals. If the observed scatter reflects primarily dihedral angle effects, the ratio of the kinetically dominant wavelength to  $\lambda_{\min}$  must depend on  $\psi$ .

While the pore spacing:pore diameter ratio determines the dominant transport mechanism, the appropriate diffusivity is calculated using the measured breakdown time and the isolated pore's radius. For surface diffusion dominated breakdown of a cylindrical pore, the breakdown time is proportional to  $\frac{r_p^4}{D_s}$ . Only when  $\psi = 180^\circ$  is the isolated pore spherical and the analysis strictly valid. For a lenticular pore on a two grain interface,  $r_p$ , the apparent pore radius, is both proportional to  $\lambda^{1/2}$  and a function of  $\psi$ . The breakdown time will also be modified by dihedral angle effects on both local curvature differences and the volume of mass which must be transported to accommodate breakdown. Discrepancies between surface diffusivities determined using single crystals and polycrystals are thus likely. A quantitative assessment of these effects is in progress.<sup>24</sup>

### 3.3. Consideration of $n = 3$

Pore stability during intermediate stage sintering has been considered by Beere,<sup>18,19</sup> Tucker and Turnbull<sup>20</sup>, as well as others. Two approaches have been employed. Beere, and Tucker and Turnbull have assumed a specific grain shape, a tetrakaidecahedron, and evaluated the pore shape minimizing the total interfacial energy (at constant density) as a function of  $\psi$ . The results indicate that the compact density at which a continuous pore phase (along three grain junctions) is no longer stable increases as  $\psi$  decreases. Pore phase breakdown is predicted at a pore fraction of  $\approx 8\%$  when  $\psi = 180^\circ$ , and a pore fraction approaching 0% as  $\psi \rightarrow 60^\circ$ . For  $\text{UO}_2$ , for which  $\psi \approx 90^\circ$  is quoted, the critical porosity is  $\approx 4\%$ . Similar values are presented by Tucker and Turnbull.

Alternatively, the pore phase has been approximated as a cylindrical channel along three grain junctions. Breakdown of the continuous pore phase, marking the transition from intermediate to final stage sintering, has been assumed to occur by perturbation growth processes.

Assuming the same grain shape as Beere, and equating the grain edge length to  $\lambda_{\min}$ , one can similarly estimate the critical density at which pore closure could occur by a Rayleigh instability. The volume fractions porosity corresponding to  $\psi = 180^\circ$ ,  $90^\circ$  and  $60^\circ$  are  $\approx 8\%$ ,  $2\%$ , and  $0\%$  respectively. Although this approach neglects "end effects" associated with four grain corners, a similar trend in stability and critical pore fraction is indicated; a decrease in  $\psi$  is expected to delay pore closure until a higher density has been reached. The dihedral angle distribution may consequently have an important modifying effect on microstructural evolution.

Nichols has recently presented a simplified model for stable open porosity in which pores are idealized as cylinders, predicting a critical volume fraction of porosity (or swelling) of  $\approx 5-6\%$  for the continuous/discontinuous porosity transition for equiaxed grains.<sup>27</sup> A dihedral angle distribution would be expected to introduce a spectrum of transition conditions, with pore channels of higher  $\psi$  closing more rapidly and at lower density. The gradual loss of (redundant) open pore channels makes gas removal (e.g., binder burnout) more difficult. Eventually, regions will become isolated from the surface due to the closure of lower  $\psi$  channels. Pore phase continuity will also affect the swelling of ceramic nuclear fuels. During swelling, low  $\psi$  channels would be expected to open first, and venting of gases should occur when adequate pore interconnectivity is achieved.

Dihedral angle distribution dependent spectra of pore closure conditions and sizes, will also introduce a spectrum of pore-grain boundary separation conditions. This factor, combined with effects of  $\psi$  on pore shrinkage and coarsening behavior, as well as pore mobility,<sup>28</sup> may contribute to the development of microstructural inhomogeneities promoting the initiation of abnormal grain growth.

Narrowing the dihedral angle distribution would be expected to lead to more uniform microstructure development. A comparison of dihedral angle measurements in undoped and MgO-doped  $\text{Al}_2\text{O}_3$ ,<sup>26</sup> has indicated that dopant additions reduce the width of the dihedral angle distribution. Handwerker et al. point out this increases the uniformity of

microstructural evolution by reducing the variation in driving forces for densification.<sup>29</sup> The potential benefits of a dopant-induced reduction in boundary mobility have frequently been cited. Dopant effects on the uniformity of the pore structure produced during the transition from intermediate to final stage sintering may also be important.

In addition to the pore phase in powder compacts, second phases at three-grain junctions are commonly found in alloys with a large difference in either the melting points or solubilities of the constituents.<sup>17</sup> A residual glassy phase along three-grain junctions may also develop in liquid-phase sintered materials. Similar stabilizing effects may be of importance in these cases as well.

#### 3.4. Consideration of $n \geq 4$

Table I illustrates the increased stability to perturbation growth accompanying an increase in  $n$  ( $\psi$  constant). The enhanced stability is manifested in two ways. The stabilizing effect becomes significant at progressively higher  $\psi$  as  $n$  increases, and the dihedral angle range within which perturbation growth is possible diminishes (Figs. 2-4). Thus, stabilization effects of the type considered are expected to be extremely important when a continuous phase is bounded by a large number of grains.

When  $n$  is large, one would also anticipate periodic fiber-matrix grain boundary intersections along the fiber axis, and "rumpling" of the fiber surface in the  $z$  direction. The resulting changes in the geometry of both the unperturbed reference state and the perturbed state are expected to modify  $\lambda_{\min}$ . Growth of a perturbation results in a net increase in grain boundary area and enhances stability (Eq. 21). Increasing grain boundary density is thus expected to increase  $\lambda_{\min}$ . The extent to which  $\lambda_{\min}$  is increased by this effect increases as  $\psi$  decreases, perhaps as much as doubling  $\lambda_{\min}$  as  $\psi \rightarrow \pi - \frac{2\pi}{n}$ . When  $\psi < 180^\circ$ , surface rumpling will also modify  $\lambda_{\min}$ , however, a quantitative assessment is difficult.

The general trend illustrated in Table I suggests that the high temperature stability of intergranular phases could be enhanced by proper manipulation of  $\psi$  and  $n$ . If stability to breakdown were desirable, e.g., fibers in composites, it would be advantageous to maximize the number of coordinating grains. Thus grain size: fiber diameter ratio ( $Q$ ) emerges as a potentially important parameter in materials design.

Grain growth and fiber coarsening may modify  $n$ , introducing an additional time-dependent component to morphological stability. Grain growth may dramatically decrease fiber stability within certain ranges of  $Q$ . A decrease in  $Q$  from 20 to 4 may only have a limited effect, whereas an additional factor of 2-3 increase in grain size would likely have a profound influence on fiber stability.

When  $n$  is sufficiently large to inhibit perturbation growth, other factors inducing mass redistribution along or between fibers may assume greater significance. A variation in  $n$  along the fiber axis will produce local curvature differences may induce mass transfer from regions of lower- $n$  to higher- $n$  regions; relatively coarse-grained regions may emerge as preferential fiber-pinchoff sites. Similarly, differences in coordination number may provide a driving force for interfiber mass transfer (coarsening).

Cline has proposed that if the rod fraction in a composite exceeds 20%, two-dimensional coarsening occurs more rapidly than breakdown and spheroidization.<sup>3</sup> Weatherly has proposed a lower volume fraction for this transition.<sup>5</sup> These estimates are likely to be further modified when intergranular phases are considered. The minimum aspect ratio necessary for breakdown into two or more particles will increase as  $n$  increases or  $\psi$  decreases. Local surface curvatures, and thus the curvature differences driving coarsening are also affected by  $n$  and  $\psi$ . Thus, analysis of transition conditions appropriate to intergranular phases is likely to be complex.

Table I is a comparison of  $\frac{\lambda}{2\pi R_c}$ ,  $\frac{\lambda}{2\pi\rho}$ , and  $\frac{\lambda}{2\pi R_{eq}}$  for  $\psi = 135^\circ$  and  $n$  varying from 2 to

8.

TABLE I			
number, $n$	$\frac{\lambda}{2\pi R_c}$	$\frac{\lambda}{2\pi\rho}$	$\frac{\lambda}{2\pi R_{eq}}$
2	0.910	0.841	1.161
3	1.093	0.768	1.266
4	1.271	0.688	1.415
5	1.500	0.596	1.633
6	1.864	0.487	2.000
7	2.663	0.344	2.824
8	$\infty$	0	$\infty$

## APPENDIX I

In this appendix, the detailed analysis of  $\lambda_{\min}$  is presented. Enough of the details are eliminated to make this appendix approach brevity and enough of the tricks are included to keep the reader on the right track; perhaps even interested.

### 1. GEOMETRY

The intersection of the grain boundaries with the surfaces form vertices of an  $n$ -sided regular polygon. The polygon is circumscribed by a circle of radius,  $R_c$ . The center of the circle coincides with the origin of a cartesian coordinate system. Local equilibrium requires each surface to have uniform curvature, let the radius of curvature for each particle be  $\rho'$ . It is always possible to arrange one of the  $n$  circles so its center lies upon  $(\xi, 0)$ , where,  $-\infty < \xi \leq 0$ . The equation for the circle is: (see fig. N)

$$(x + \eta')^2 + y^2 = \rho'^2 \quad (\text{IA-1})$$

from the law of sines,

$$\frac{\rho'}{\sin(\frac{\pi}{n})} = \frac{\eta'}{\cos(\frac{\psi}{2})} = -\frac{R_c}{\cos(\frac{\pi}{n} + \frac{\psi}{2})} \quad (\text{IA-2})$$

Define

$$\rho \equiv \frac{\rho'}{R_c} \quad \text{and} \quad \eta \equiv \frac{\eta'}{R_c} \quad (\text{IA-3})$$

Transforming to cylindrical coordinates and restricting  $r$  to the surface. ( $x \rightarrow r \cos \theta$ ,  $y \rightarrow r \sin \theta$ ,  $z \rightarrow z$ )

$$r = R_c(\rho^2 - \eta^2 \sin^2 \theta)^{1/2} \quad (\text{IA-4})$$

We perturb the circumscribing circle infinitesimally

$$R_c = R_o + \delta \cos kz \quad (\text{IA-5})$$

where  $\delta$  is an arbitrarily small amplitude and  $k \equiv \frac{2\pi}{\lambda}$  is the wavenumber of a fourier mode.

Equations (4) and (5) give:

$$r = (R_o + \delta \cos kz)[- \eta \cos \theta + (\rho^2 - \eta^2 \sin^2 \theta)^{1/2}] \quad (\text{IA-6})$$

Noting that  $\rho$  and  $\eta$  are not functions of  $z$ , we define:

$$r = r_\theta r_z \quad (\text{IA-7})$$

where

$$r_z = R_o + \delta \cos kz \quad \text{and} \quad r_\theta = -\eta \cos \theta + (\rho^2 - \eta^2 \sin^2 \theta)^{1/2} \quad (\text{IA-8})$$

## 2. Thermodynamics

The surface free energy is:

$$F = \sum_i \gamma_i \sigma_i \quad (\text{IA-9})$$

where  $\gamma_i$  is the specific surface energy of the  $i^{\text{th}}$  surface and  $\sigma_i$  is the total area of the  $i^{\text{th}}$  surface.

For the case at hand,

$$F = \gamma_s \sigma_s + \gamma_{gb} \sigma_{gb} \quad (\text{IA-10})$$

It is sufficient to consider only the surface energy per wavelength, defining  $f = \frac{F}{\lambda}$ :

$$f = \gamma_s A_s + \gamma_{gb} A_{gb} \quad (\text{IA-11})$$

## 3. CALCULUS

Calculating  $A_{gb}$  first:

$$A_{gb} = n \int_0^{\frac{2\pi}{k}} dz [\alpha - (R_o + \delta \cos kz)] \quad (\text{IA-12})$$

where  $\alpha$  is an arbitrary length.

$$A_{gb} = \frac{2n\pi}{k}(\alpha - R_o) \quad (\text{IA-13})$$

Now for  $A_s$

$$A_s = n \int_{-\frac{\pi}{n}}^{\frac{\pi}{n}} d\theta \int_0^{\frac{2\pi}{k}} dz \left[ r^2 + \left( \frac{\partial r}{\partial \theta} \right)^2 + r^2 \left( \frac{\partial r}{\partial z} \right)^2 \right]^{1/2} \quad (\text{IA-14})$$

rearranging

$$A_s = n \int_{-\frac{\pi}{n}}^{\frac{\pi}{n}} d\theta \int_0^{\frac{2\pi}{k}} dz \left[ r^2 + \left( \frac{\partial r}{\partial \theta} \right)^2 \right]^{1/2} \left[ 1 + \frac{r^2 \left( \frac{\partial r}{\partial z} \right)^2 r^2}{r^2 + \left( \frac{\partial r}{\partial \theta} \right)^2} \right]^{1/2} \quad (\text{IA-15})$$

Note that  $\left( \frac{\partial r}{\partial z} \right)$  is of order  $\delta$ . We shall call sufficient approximation any taylor series up to and including order  $\delta^2$ . To sufficient approximation then:

$$A_s = n \int_{-\frac{\pi}{n}}^{\frac{\pi}{n}} d\theta \int_0^{\frac{2\pi}{k}} dz \left[ r^2 + \left( \frac{\partial r}{\partial \theta} \right)^2 \right]^{1/2} \left[ 1 + \frac{r^2 \left( \frac{\partial r}{\partial z} \right)^2 r^2}{2(r^2 + \left( \frac{\partial r}{\partial \theta} \right)^2)} \right] \quad (\text{IA-16})$$

using (7) and factoring,

$$A_s = n \int_{-\frac{\pi}{n}}^{\frac{\pi}{n}} d\theta \int_0^{\frac{2\pi}{k}} dz (R_o + \delta \cos kz) \left[ r_\theta^2 + \left( \frac{dr_\theta}{d\theta} \right)^2 \right]^{1/2} \left[ 1 + \frac{r_\theta^4 \delta^2 k^2 \sin^2 kz}{2(r_\theta^2 + \left( \frac{dr_\theta}{d\theta} \right)^2)} \right] \quad (\text{IA-17})$$

Again to sufficient approximation,

$$A_s = n \int_{-\frac{\pi}{n}}^{\frac{\pi}{n}} d\theta \left[ r_\theta^2 + \left( \frac{dr_\theta}{d\theta} \right)^2 \right]^{1/2} \int_0^{\frac{2\pi}{k}} dz \left\{ R_o + R_o \left[ \frac{r_\theta^4 \delta^2 k^2 \sin^2 kz}{2(r_\theta^2 + \left( \frac{dr_\theta}{d\theta} \right)^2)} \right] + \delta \cos kz \right\} \quad (\text{IA-18})$$

Integrating the z dependent part,

$$A_s = \frac{2n\pi R_o}{k} \int_{-\frac{\pi}{n}}^{\frac{\pi}{n}} d\theta \left[ r_\theta^2 + \left( \frac{dr_\theta}{d\theta} \right)^2 \right]^{1/2} \left[ 1 + \frac{\delta^2 k^2 r_\theta^4}{4(r_\theta^2 + \left( \frac{dr_\theta}{d\theta} \right)^2)} \right] \quad (\text{IA-19})$$

It is convenient to examine the term:  $r_\theta^2 + \left( \frac{dr_\theta}{d\theta} \right)^2$ .

$$\left( \frac{dr_\theta}{d\theta} \right) = \eta \sin\theta - \frac{\eta^2 \sin\theta \cos\theta}{(\rho^2 - \eta^2 \sin^2\theta)^{1/2}} \quad (\text{IA-20})$$

and after some algebra,

$$\left( \frac{dr_\theta}{d\theta} \right) = \frac{\eta r_\theta \sin\theta}{r_\theta + \eta \cos\theta} \quad (\text{IA-21})$$

With even more algebra, we find:

$$r_\theta^2 + \left( \frac{dr_\theta}{d\theta} \right)^2 = \frac{\rho^2 r_\theta^2}{(r_\theta + \eta \cos\theta)^2} \quad (\text{IA-22})$$

Rewriting equation (19),

$$A_s = \frac{2n\pi R_o}{k} \int_{-\frac{\pi}{n}}^{\frac{\pi}{n}} d\theta \left[ \frac{\rho r_\theta}{r_\theta + \eta \cos\theta} \right] \left[ 1 + \frac{\delta^2 k^2 r_\theta^4 (r_\theta + \eta \cos\theta)^2}{4\rho^2 r_\theta^2} \right] \quad (\text{IA-23})$$

with the following definitions, we have:

$$A_s = \frac{2n\pi R_o}{k} \left[ U + \frac{\delta^2 k^2}{4} P \right] \quad (\text{IA-24})$$

where

$$U = \int_{-\frac{\pi}{n}}^{\frac{\pi}{n}} d\theta \frac{\rho r_\theta}{r_\theta + \eta \cos\theta} \quad (\text{IA-25})$$

and

$$P = \int_{-\frac{\pi}{n}}^{\frac{\pi}{n}} d\theta \frac{r_\theta^3 (r_\theta + \eta \cos \theta)}{\rho} \quad (\text{IA-26})$$

Calculating U,

$$U = \rho \int_{-\frac{\pi}{n}}^{\frac{\pi}{n}} d\theta \left[ 1 - \frac{\eta \cos \theta}{(\rho^2 - \eta^2 \sin^2 \theta)^{1/2}} \right] \quad (\text{IA-27})$$

it is not too hard to find:

$$U = 2\rho \left[ \frac{\pi}{n} - \sin^{-1} \left( \frac{\eta \sin(\frac{\pi}{n})}{\rho} \right) \right] \quad (\text{IA-28})$$

Using equations (2) and (3),

$$\frac{\eta}{\rho} = \frac{\cos(\frac{\psi}{2})}{\sin(\frac{\pi}{n})} \quad (\text{IA-29})$$

we find,

$$U = 2\rho \left[ \frac{\pi}{n} - \frac{\pi}{2} + \frac{\psi}{2} \right] \quad (\text{IA-30})$$

It is convenient to split P into five parts:

$$P = P_1 + P_2 + P_3 + P_4 + P_5 \quad (\text{IA-31})$$

where

$$P_1 = -2\eta^3 \int_0^{\frac{\pi}{n}} d\theta \cos^3 \theta \left[ 1 - \frac{\eta^2 \sin^2 \theta}{\rho^2} \right]^{1/2} \quad (\text{IA-32})$$

$$P_2 = -6\eta\rho^2 \int_0^{\frac{\pi}{n}} d\theta \cos\theta \left[ 1 - \frac{\eta^2 \sin^2\theta}{\rho^2} \right]^{1/2} \quad (\text{IA-33})$$

$$P_3 = 2 \int_0^{\frac{\pi}{n}} d\theta (\rho^3 + 3\rho\eta^2) \quad (\text{IA-34})$$

$$P_4 = -\frac{2}{\rho} \int_0^{\frac{\pi}{n}} d\theta (3\eta^4 + 5\eta^2\rho^2) \sin^2\theta \quad (\text{IA-35})$$

and

$$P_5 = 8 \frac{\eta^4}{\rho} \int_0^{\frac{\pi}{n}} d\theta \sin^4\theta \quad (\text{IA-36})$$

After some simplification, the following are obtained:

$$P_1 = -2\eta^3 \left\{ \frac{2[1 + \cos^2(\frac{\pi}{n})] + \frac{\rho^2}{\eta^2}}{8} \sin(\frac{\psi}{2}) \sin(\frac{\pi}{n}) + \left[ \frac{\rho}{2\eta} + (\frac{\rho}{2\eta})^2 \right] (\frac{\pi}{2} - \frac{\psi}{2}) \right\} \quad (\text{IA-37})$$

$$P_2 = -\frac{3\eta\rho^2}{4} \left\{ \left[ 5 - 2 \frac{\eta^2 \sin^2(\frac{\pi}{n})}{\rho^2} \right] \sin(\frac{\psi}{2}) \sin(\frac{\pi}{n}) + 3 \frac{\rho}{\eta} (\frac{\pi}{2} - \frac{\psi}{2}) \right\} \quad (\text{IA-38})$$

$$P_3 = (2\rho^3 + 6\eta^2\rho) \frac{\pi}{n} \quad (\text{IA-39})$$

$$P_4 = \left[ \frac{3\eta^4}{\rho} + 5\eta^2\rho \right] \left[ \sin(\frac{\pi}{n}) \cos(\frac{\pi}{n}) - \frac{\pi}{n} \right] \quad (\text{IA-40})$$

$$P_5 = \frac{\eta^4}{\rho} \left[ 3 \frac{\pi}{n} - 3 \sin(\frac{\pi}{n}) \cos(\frac{\pi}{n}) - 2 \sin^3(\frac{\pi}{n}) \cos(\frac{\pi}{n}) \right] \quad (\text{IA-41})$$

Combining equations (37) through (41) with the definition, (31), and simplifying, we get for P:

$$P = (2\rho^3 + \rho\eta^2)\left(\frac{\pi}{n} + \frac{\psi}{2} - \frac{\pi}{2}\right) + \quad (\text{IA-42})$$

$$\cos\left(\frac{\psi}{2}\right)\left(5\eta\rho^2\cos\left(\frac{\pi}{n}\right) - 2\eta^3\sin^2\left(\frac{\pi}{n}\right)\cos\left(\frac{\pi}{n}\right) - \eta^2\rho\sin\left(\frac{\psi}{2}\right) - 2\rho^3\sin\left(\frac{\psi}{2}\right) - 2\rho^3\sin^3\left(\frac{\psi}{2}\right)\right)$$

#### 4. VOLUME DETERMINATION

Simple geometry yields the following expression for the cross-sectional area

$$A(z) = nR_c^2 \left[ \sin\left(\frac{\pi}{n}\right)\cos\left(\frac{\pi}{n}\right) + \sin\left(\frac{\psi}{2} + \frac{\pi}{n}\right)\cos\left(\frac{\psi}{2} + \frac{\pi}{n}\right) + \frac{\psi}{2} + \frac{\pi}{n} - \frac{\pi}{2} \right] \quad (\text{IA-43})$$

using the definition for  $R_c$ , and defining a scaling factor  $V_u$ :

$$A(z) = (R_o^2 + 2R_o\delta\cos kz + \delta^2\cos^2 kz)V_u \quad (\text{IA-44})$$

The volume per wavelength of the perturbed shape is:

$$V_p = \int_0^{\frac{2\pi}{k}} dz A(z) \quad (\text{IA-45})$$

integrating,

$$V_p = \frac{\pi V_u}{k} (2R_o^2 + \delta^2) \quad (\text{IA-46})$$

#### 5. ANALYSIS

Since,

$$\gamma_{gb} = 2\gamma_s \cos\left(\frac{\psi}{2}\right) \quad (\text{IA-47})$$

(11) becomes:

$$f = \gamma_s (A_s + 2\cos\left(\frac{\psi}{2}\right)A_{gb}) \quad (\text{IA-48})$$

with (13) and (24):

$$f = \gamma_s \frac{2n\pi}{k} \left\{ \left[ U + \frac{\delta^2 k^2 P}{4} - 2\cos\left(\frac{\psi}{2}\right) \right] R_o + 2\alpha \cos\left(\frac{\psi}{2}\right) \right\} \quad (\text{IA-49})$$

Solving (46) for  $R_o$ ,

$$R_o = \left[ \frac{kV_p}{2\pi V_u} \right]^{1/2} \left[ 1 - \frac{\pi V_u}{kV_p} \delta^2 \right]^{1/2} \quad (\text{IA-50})$$

to sufficient approximation:

$$R_o = \left[ \frac{kV_p}{2\pi V_u} \right]^{1/2} - \left[ \frac{2\pi V_u}{kV_p} \right]^{1/2} \frac{\delta^2}{4} \quad (\text{IA-51})$$

using (51) in the expression (49) and simplifying,

$$f = \gamma_s \left[ \frac{4n\pi \cos\left(\frac{\psi}{2}\right) \alpha}{k} + \frac{2n\pi}{k} \left[ \frac{kV_p}{2\pi V_u} \right]^{1/2} U - \frac{4n\pi \cos\left(\frac{\psi}{2}\right) \alpha}{k} \cos\left(\frac{\psi}{2}\right) \left[ \frac{kV_p}{2\pi V_u} \right]^{1/2} \right] + \quad (\text{IA-52})$$

$$\gamma_s \frac{n\pi}{k} \left[ \frac{kV_p}{2\pi V_u} \right]^{1/2} \left[ 2\cos\left(\frac{\psi}{2}\right) - U + \left[ \frac{kV_p}{2\pi V_u} \right] k^2 P \right] \frac{\delta^2}{2}$$

If the term which multiplies  $\delta^2$  is positive, the free energy is increased by the perturbation; conversely, a perturbation grows if

$$2\cos\left(\frac{\psi}{2}\right) - U + Pk^2 \left[ \frac{kV_p}{2\pi V_u} \right] < 0 \quad (\text{IA-53})$$

Since we need only determine the sign for expressions like the above, it is valid to write:

$$\frac{kV_p}{2\pi V_u} = R_o^2 \quad (\text{IA-54})$$

For all perturbations for which  $\lambda > \lambda_{\min}$ , where,

$$\lambda_{\min} = 2\pi R_o \left[ \frac{P}{U - 2\cos\left(\frac{\psi}{2}\right)} \right]^{1/2} \quad (\text{IA-55})$$

amplitudes will increase with time.

## Appendix II: End-State Calculation

It is useful to determine the size of the discrete particle, resulting from the breakup of a continuous phase, which yields the same total interfacial energy as the original unperturbed continuous phase. The calculated size defines an absolute lower limit for the wavelength of breakup, independent of the perturbation details. A sample calculation for  $n = 2$  is presented below.

Using parameters defined in appendix I, the volume of the continuous phase assumes the form:

$$V_c = \frac{\psi - \sin(\psi)}{\sin^2(\frac{\psi}{2})} \lambda R_o^2 \quad (\text{IIA-1})$$

The total interfacial energy is given by:

$$f_c = 4\cos(\frac{\psi}{2})\lambda(\alpha - R_o) + \frac{2\psi}{\sin(\frac{\psi}{2})} \lambda R_o \quad (\text{IIA-2})$$

In eq. IIA-2, the first term is due to the boundary and scales with the factor  $2\cos\frac{\psi}{2}$ , since  $\gamma_s$  has been set to unity.

The volume of the discrete phase is:

$$V_d = \frac{2\pi}{3} [2 + \cos(\frac{\psi}{2})][1 - \cos(\frac{\psi}{2})]^2 r^3 \quad (\text{IIA-3})$$

where  $r$  is the radius of curvature of the spherical cap.

The total interfacial energy for the discrete phase is

$$f_d = 2\cos(\frac{\psi}{2})[2\alpha\lambda - \pi r^2 \sin^2(\frac{\psi}{2})] + 4\pi[1 - \cos(\frac{\psi}{2})]r^2 \quad (\text{IIA-4})$$

Volume conservation requires that  $V_c = V_d$ . The lower limit wavelength  $\lambda_{ll}$  is thus defined by setting  $f_c = f_d$ , yielding

$$\frac{\lambda_{ll}}{2\pi R_o} = \frac{9 \left\{ 2[1 - \cos(\frac{\psi}{2})] - \cos(\frac{\psi}{2})\sin^2(\frac{\psi}{2}) \right\}^3}{[8\sin(\frac{\psi}{2})][\psi - \sin(\psi)][2 + \cos(\frac{\psi}{2})]^2 [1 - \cos(\frac{\psi}{2})]^4} \quad (\text{IIA-5})$$

The limit of  $\frac{\lambda_{II}}{2\pi R_o}$  as  $\psi$  approaches 0 is  $(\frac{3^4}{2^7})$  which is  $\approx 0.6328$ .

**Appendix III: Effect of  $\psi$  on  $\frac{\lambda}{2r_p}$**

Crack healing experiments have been employed to estimate the surface diffusivity of alumina. The transport mechanism controlling breakdown of high aspect ratio pore channels is determined by evaluating the pore spacing:pore diameter ratio. An analysis of dihedral angle effects on this ratio for  $n = 2$  follows.

The volume conservation condition  $V_c = V_d$  (Appendix II) provides a relationship between  $R_o$  and  $r$ . The spacing between pore centers is simply  $\lambda$ . The apparent (grain boundary plane) pore radius  $r_p$  is related to the radius of curvature of the spherical cap  $r$  by

$$r_p = r \sin\left(\frac{\psi}{2}\right) \quad \text{(IIIA-1)}$$

If the perturbation wavelength is expressed as

$$\lambda = \kappa 2\pi R_o \quad \text{(IIIA-2)}$$

where  $\kappa$  is a kinetic scaling factor, the ratio  $\frac{\lambda}{2r_p}$  is of the form

$$\frac{\lambda}{2r_p} = C \kappa^{\frac{2}{3}} [G(\psi)]^{\frac{1}{3}} \quad \text{(IIIA-3)}$$

where

$$G(\psi) = \frac{2 - 3\cos\left(\frac{\psi}{2}\right) + \cos^3\left(\frac{\psi}{2}\right)}{\sin\left(\frac{\psi}{2}\right)[\psi - \sin(\psi)]} \quad \text{(IIIA-4)}$$

Consequently, to assess the changes in  $\frac{\lambda}{2r_p}$  that are purely the consequence of changes in phase geometry, one can evaluate the change in  $G^{\frac{1}{3}}$  as  $\psi$  varies from  $\pi$  to 0. The results are given in table II.

Table II illustrates pore spacing ratio as affected by geometry, see appendix III for clarification.

TABLE II					
$\psi$	180°	160°	140°	120°	100°
$n$	0.860	0.850	0.843	0.838	0.833
$\psi$	80°	60°	40°	20°	0°
$n$	0.830	0.828	0.827	0.826	0.825

## REFERENCES

1. Lord Rayleigh, "On the Instability of Jets," Proc. London Math. Soc., 10, 4-13 (1879)
2. Lord Rayleigh, Theory of Sound, Vol. 2, 2nd Edition, MacMillan and Co., London, (1929).
3. H. E. Cline, "Shape Instabilities of Eutectic Composites at Elevated Temperatures," Acta Metall., 19, [6], 481-90 (1971).
4. T. H. Courtney, "Thermal and Mechanical Stability in Finely Divided Structures," in New Developments and Applications in Composites, edited by D. Kuhlmann-Wilsdorf and W. C. Harrison Jr., Met. Soc. of the AIME, Warrendale PA, 1979, pp. 1-30.
5. G. C. Weatherly, "The Stability of Eutectic Microstructures at Elevated Temperatures," pp. 121-75 in Treatise on Materials Science and Technology, Vol. 8, (Academic Press, New York) (1975).
6. A. J. Stapley and C. J. Beevers, "The stability of sapphire whiskers in nickel at elevated temperatures, Part 2," J. Mater. Sci., 8, 1296-1306 (1973).
7. M. McLean, "The kinetics of spheroidization of lead inclusions in aluminium," Philos. Mag., 27, 1253-66 (1973).
8. D. M. Moon and R. C. Koo, "Mechanism and Kinetics of Bubble Formation in Doped Tungsten," Met. Trans., 2, [8], 2115-22 (1971).

9. F. A. Nichols and W. W. Mullins, "Surface (Interface) and Volume-Diffusion Contributions to Morphological Changes Driven by Capillarity," *Trans. A.I.M.E.*, 233, [10], 1840-48 (1965).
10. F. A. Nichols and W. W. Mullins, "Morphological Changes of a Surface of Revolution due to Capillarity-Induced Surface Diffusion," *J. Appl. Phys.*, 36, [6], 1826-35 (1965).
11. T. K. Gupta, "Instability of Cylindrical Voids in Alumina," *J. Am. Ceram. Soc.*, 61, [5-6], 191-95 (1978).
12. T. K. Gupta, "Crack Healing in Thermally Shocked MgO," *ibid.*, 58, [3-4], 143 (1975).
13. C. F. Yen and R. L. Coble, "Spheroidization of Tubular Voids in  $Al_2O_3$  Crystals at High Temperatures," *ibid.*, 55, [10], 507-09 (1972).
14. O. Maruyama and W. Komatsu, "Observations on the Grain-Boundary of  $Al_2O_3$  Bicrystals," *Ceramurgica International*, 5, [2], 51-5 (1979).
15. W. C. Carter and A. M. Glaeser, "Dihedral Angle Effects on the Stability of Pore Channels," *J. Am. Ceram. Soc.*, 67, [6], C124-C127 (1984).
16. M. D. Drory and A. M. Glaeser, "The Stability of Pore Channels: Experimental Observations," *ibid.*, 68, [1], C14-C15 (1985).
17. C. S. Smith, "Grains, Phases, and Interfaces: An Interpretation of Microstructure," *Trans. A.I.M.E.*, 175, [1], 15-51 (1948).

18. W. Beere, "A Unifying Theory of the Stability of Penetrating Liquid Phases and Sintering Pores," *Acta Metall.*, 23, [1], 131-8 (1975).
19. W. Beere, "The sintering and morphology of interconnected porosity in  $UO_2$  powder compacts," *J. Mat. Sci.*, 8, [12], 1717-24 (1973).
20. M. O. Tucker and J. A. Turnbull, "The morphology of interlinked porosity in nuclear fuels," *Proc. R. Soc. Lond. A.* 343, 299-314 (1975).
21. F. A. Nichols, "On the Spheroidization of Rod-Shaped Particles of Finite Length," *J. Mater. Sci.*, 11, [6], 1077-82 (1976).
22. J. W. Cahn, "Stability of Rods with Anisotropic Surface Free Energy," *Scripta Metall.*, 13, [11], 1069-71 (1979).
23. W. C. Carter and A. M. Glaeser, "The Morphological Stability of Continuous Intergranular Phases," to be published in *Proceedings of the Twenty-First University Conference on Ceramic Science, Penn State University, July 17-19, 1985 (also LBL Report #19160)*.
24. W. C. Carter and A. M. Glaeser, to be published.
25. P. J. Clemm and J. C. Fisher, "The Influence of Grain Boundaries on the Nucleation of Secondary Phases," *Acta Metall.*, 3, [1], 70-73 (1955).

26. C. A. Handwerker, "Sintering and Grain Growth in MgO"; Sc.D. Thesis, Massachusetts Institute of Technology, Cambridge, MA, February 1983.
  
27. F. A. Nichols, "A Simplified Model for Stable Open Porosity," submitted to J. Am. Ceram. Soc..
  
28. C. H. Hsueh, A. G. Evans, and R. L. Coble, "Microstructure Development During Final/Intermediate Stage Sintering - I. Pore/Grain Boundary Separation," Acta Metall., 30, [7], 1269-79 (1982).
  
29. C. A. Handwerker, R. M. Cannon, and R. L. Coble, "Final Stage Sintering of MgO," pp. 619-43 in Structure and Properties of MgO and Al<sub>2</sub>O<sub>3</sub> Ceramics, Vol. 23 in Advances in Ceramics, W. D. Kingery, Ed., ACS Publication (1984).

LAWRENCE BERKELEY LABORATORY  
TECHNICAL INFORMATION DEPARTMENT  
UNIVERSITY OF CALIFORNIA  
BERKELEY, CALIFORNIA 94720